Remote Sensing Applications: Society and Environment 34 (2024) 101192

Contents lists available at ScienceDirect

Remote Sensing Applications: Society and Environment

journal homepage: www.elsevier.com/locate/rsase

Perennial snow and ice cover change from 2001 to 2021 in the Hindu-Kush Himalayan region derived from the Landsat analysis-ready data

Ahmad Khan [a, *], Peter Potapov [a], Matthew C. Hansen [a], Amy H. Pickens [a], Alexandra Tyukavina [a], Andres Hernandez Serna [a], Kabir Uddin [b], Jawairia Ahmad [c]

[a] *Department of Geographical Sciences, University of Maryland, College Park, MD, 20742, USA*
[b] *ICIMOD, Kathmandu, Nepal*
[c] *Centre for Water Informatics and Technology, SBA School of Science and Engineering, Lahore University of Management Sciences (LUMS), Lahore, Pakistan*

ARTICLE INFO

Keywords:
Landsat
Perennial snow and ice
Hindu-kush Himalayas
glaciers
Snowfields
Climate change

ABSTRACT

The changing climate directly affects spatial and temporal patterns of snow and ice cover globally and in the Hindu-Kush Himalayan (HKH) region. In the HKH, around 3.3 billion people across 11 countries depend on water originating from mountain glaciers and snowfields, and melting snow cover has a direct impact on their livelihood and well-being. Various studies have shown that the snow and ice cover in the HKH is declining at an alarming rate but have been limited in geographic, spatial and temporal scales. Here, we employed the Global Land Analysis and Discovery analysis ready Landsat time-series data (GLAD ARD) to map changes in perennial snow and ice between 2001 and 2021 at five-year epochs using decision tree ensemble models. These maps were used to create a stratified sampling design for reference data collection to estimate area and map accuracy. All five-year epoch maps have user's accuracies above 90% and producer's accuracies above 91%. Our sample data analysis showed that one-eighth of the extent of perennial snow and ice in the HKH, totalling 15,770 km^2 (CI ± 3195 km^2), disappeared over the last two decades with 105,935 km^2 (CI ± 3396 km^2) remaining in 2021. From map-based estimates, the largest decline of perennial snow and ice cover among the mountain ranges was found in the Himalayas with an estimated reduction of 5741 km^2. Among HKH countries, China had the largest area of perennial snow and ice reduction of 10,654 km^2, Nepal had the highest net perennial snow and ice reduction rate (31%). Among the river basins, the maximum net loss of perennial snow and ice cover between 2001 and 2021 was in the Indus (24.8%), followed by Brahmaputra (18.3%), and Tarim (15.7%). Our results confirm wide-spread loss of perennial snow and ice across the HKH region and provide both regionally consistent maps with derived area estimates at landform, national and basin-levels and methodology to continue monitoring snow and ice melt.

* Corresponding author.
E-mail addresses: akhan234@umd.edu (A. Khan), potapov@umd.edu (P. Potapov), mhansen@umd.edu (M.C. Hansen), ahudson2@umd.edu (A.H. Pickens), atyukav@umd.edu (A. Tyukavina), Kabir.Uddin@icimod.org (K. Uddin), jawairia.ahmad@lums.edu.pk (J. Ahmad).

https://doi.org/10.1016/j.rsase.2024.101192
Received 11 November 2023; Received in revised form 23 December 2023; Accepted 20 March 2024
Available online 22 March 2024

1. Introduction

The Hindu Kush Himalayan (HKH) region (Fig. 1) is one of the major glaciated regions outside polar zones with a substantial extent of seasonal and perennial snow and ice cover (Erickson 1984; Owen et al., 2002). The snowfields, ice sheets, and glaciers of the HKH region provide major contribution to the flows for the nine major river basins originating in the region (Bookhagen and Burbank 2010; Immerzeel et al., 2009). In particular, snow and ice melt contribute 40% and 32%, respectively, to stream flows in the upper Indus Basin (Immerzeel et al., 2009). The rivers originating in the HKH region characterize regional ecosystems, support biodiversity, and provide various ecosystem services for the downstream populations (Bajracharya and Shrestha 2011). The livelihoods of the 3.3 billion people (WorldBank 2023) who inhabit the HKH rivers basins in 11 countries (Wester et al., 2019) depend on water provided by snow and ice melt (Bajracharya and Shrestha 2011). A significant negative change in the hydrological balance of HKH will have disastrous consequences for the region and the downstream communities.

The changing climate has substantial impact on the perennial and seasonal snow cover in the HKH region (Immerzeel et al., 2010). Glaciers of the HKH region are retreating faster than the global average (Dyurgerov and Meier 2005) with an acceleration of glacial mass loss by 65% in 2010–2019 (Wester et al., 2023). Lee et al. (2021) reported a 40% reduction in the Himalayan glacier cover over the last four decades. Change in glacial mass loss in the HKH region is alarming as it changed from an annual 0.17 m water quality (m.w.e) for 2000–2009 to −0.28 m.w.e. per year for 2010–2019 (Wester et al., 2023). Although it is difficult to estimate snow cover due to seasonal and inter-annual variations (Desinayak et al., 2022), there is a consensus that the snow cover of HKH is shrinking (IPCC 2022) with an average decline of five snow cover days per decade (Wester et al., 2023). It is projected that snow cover in the HKH will reduce by between 1% and 26% for an average rise in temperature between 1.5 °C and 4 °C (Wester et al., 2023).

The temperature of the Himalayan region showed warming trends of +0.28 °C on average per decade for the period 1951–2020 (Wester et al., 2023), which is significantly higher than the previously reported trend of +0.12 °C per decade from 1971 to 1994 (Shrestha et al., 1999) and 0.104 °C mean temperature rise per decade from 1901 to 2014 (Ren et al., 2017). Tibetan Plateau shows a higher warming trend than the average across the HKH with +0.45 °C ± 0.09 °C per decade during 1980–2018 (Peng et al., 2021). The warming trend in the HKH is alarming in comparison to the rise in Earth's temperature of 0.14 °C–0.20 °C per decade since 1880 (Lindsey et al., 2023; NASA 2023; Shrestha et al., 2015). Viste and Sorteberg (2015) projected temperature to increase by 4.9–6.2 °C in the Indus, 3.6–5.2 °C in the Ganges, and 4.2–6.0 °C in the Brahmaputra river basins during 2071–2100.

By 2021, a glacier mass loss of 18 ± 13% is expected resulting in a 20% decrease in water availability for irrigation in dependent river basins (Bolch et al., 2012; IPCC et al., 2022b). It is projected that glaciers in HKH region will lose 30%–50% of their volume by 2100 for a 1.5 °C–2 °C rise in global warming (Wester et al., 2023). Even a 1.5 °C increase in global temperature will affect communities in river basins that depend on ice and snow melt (IPCC et al., 2007; 2022b) with the associated reduction in the contribution of snow and ice melt to the river flow in the HKH having catastrophic impacts on the agricultural irrigation system (Archer 2001, 2003).

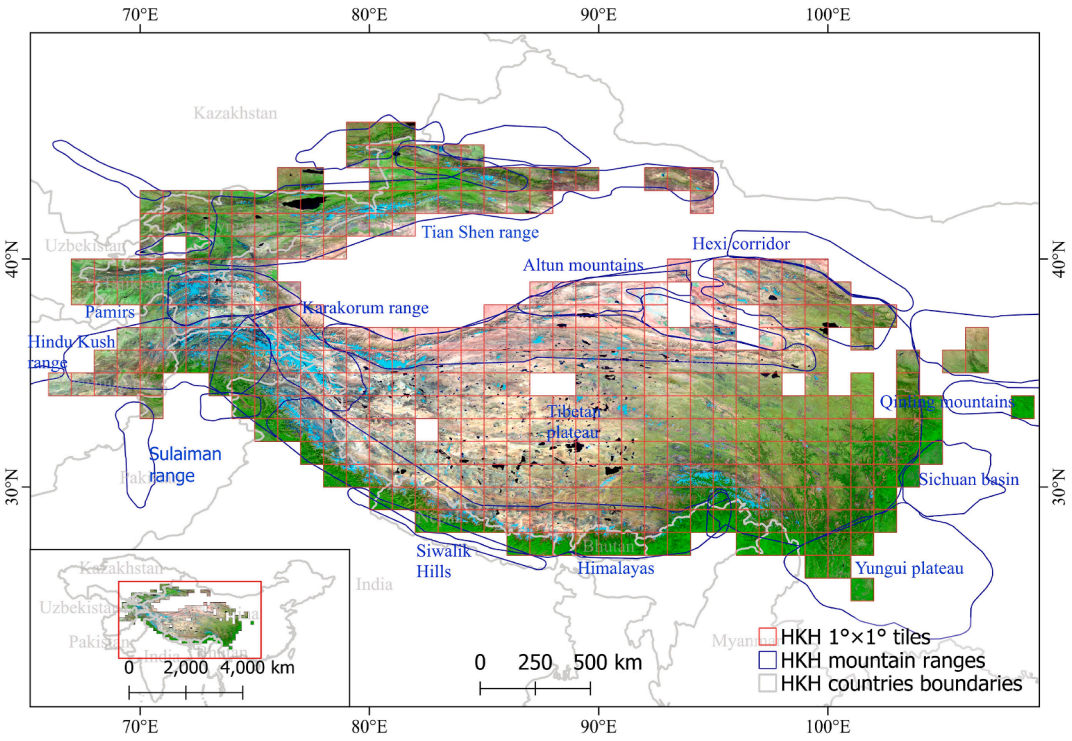

Fig. 1. Study area of Hindu Kush Himalaya region. The background image is the Landsat ARD clear-sky image composite for the year 2021, band combination of SWIR-NIR-red.

Consistent estimates of the area, spatial extent, and changes in perennial snow and ice cover for the HKH region are required to quantify the direct impact of climate change (Remy et al., 2012; Shrestha et al., 2015). This potentially catastrophic impact calls for monitoring of the snow cover dynamics in the HKH region.

Satellite remote sensing offers an alternative to conventional surveying for mapping and monitoring snow ice cover change providing information that is difficult to collect with in-situ conventional tools (Desinayak et al., 2022). Monitoring snow cover with in-situ conventional methods dates back to the 1800s in eastern China (Brown 2000) but is geographically limited to date by access and logistical constraints. The terrain of HKH is highly rugged and complex, remote, and difficult to access for physical surveying (Bolch et al., 2012; Shrestha et al., 2015). Continental-scale remote sensing was adopted by the US National Oceanic and Atmospheric Administration (NOAA) in 1966 with the launch of a weekly analysis of snow and ice cover using visible satellite imagery (Hall et al., 2002; Matson et al., 1986). Snow cover monitoring with satellite data in HKH started in 1976 with mapping of snow cover for Sutlej and Beas Basins, which are tributaries of the Indus, using the Advanced Very High Resolution Radiometer (AVHRR) data (Ramamoorthi and Haefner 1991). The Moderate Resolution Imaging Spectroradiometer (MODIS) global snow extent data at 500 m spatial resolution have been supporting snow and ice monitoring since 2000 (Hall et al., 2002). Few estimates of the snow cover extent and change over time for the HKH region have been derived from coarse spatial resolution (≥250 m) data (Desinayak et al., 2022; Gurung et al., 2011a; Shrestha et al., 2015). Gurung et al. (2011b) estimated perennial snow cover as 2% of the total HKH land cover area using an 8-day MODIS snow cover product for 2001–2010. Studies employing MODIS and AVHRR data have demonstrated a declining snow and ice cover in the Tibetan Plateau (Wang et al., 2015) and in the Himalayan region (Cogley 2016; Gurung et al., 2011b; Immerzeel 2008; Pratibha and Kulkarni 2018; Rikiishi and Nakasato 2006; Wang and Xie 2009).

However, these coarse resolution snow and ice products suffer from high uncertainty. For example, the overall accuracy of MODIS-based snow cover map for the HKH by Gurung et al. (2011a) ranged between 46.2% and 97.3% over different months. The high uncertainty of coarse resolution snow and ice products may affect the monitoring of such a spatially rare class (Racoviteanu et al., 2009). The minimal annual snow and ice extent observed at a given spatial resolution can be labelled as the "perennial snow cover" (Trishchenko and Ungureanu 2021).

Higher spatial resolution data such as the Landsat data offers an opportunity to map perennial snow and ice with lower spatial uncertainty. At the same time, the low historic (pre-2013) frequency of clear-sky Landsat data observations in the mountain area does not support annual mapping of perennial snow cover (Zhou et al., 2019). Thus, the change in perennial snow and ice cover extent is difficult to assess given inter- and intra-annual spatial and temporal variability in snow accumulation and melting.

The goal of the current study was to assess the extent of perennial snow and ice cover and its changes over time in the HKH region from 2001 to 2021 at the spatial resolution of 30 m. The first objective was to map perennial snow and ice extent regionally at five-year epochs using the Landsat optical time-series data from 1997 to 2021. In this research, we employed the Landsat analysis ready (ARD) data (Potapov et al., 2020) provided by the Global Land Analysis and Discovery (GLAD) team at the University of Maryland. GLAD ARD were aggregated into five intervals 1997–2001, 2002–2006, 2007–2011, 2012–2016, and 2017–2021, referred heretofore to as 2001, 2006, 2011, 2016, and 2021 epoch, respectively. The mapping method was decision tree ensembles calibrated with manually collected training data. Our second objective was to estimate the area of snow and ice cover and change with a probability sample of reference data together with the accuracy of the five-year epoch maps. Using our map and sample data, we characterized the multi-decadal changes of the perennial snow and ice cover within the entire HKH region and its mountain systems, river basins, and countries. The methodology and map time-series developed by the GLAD team at UMD and presented here are employed as part of the Regional Land Cover Monitoring System (RLCMS) by the International Centre for Integrated Mountains Development (ICIMOD) under the SERVIR-Hindu Kush Himalaya project funded by the National Aeronautics and Space Administration (NASA).

2. Data and methods

2.1. Geographic extent

The focus of this study is the Hindu Kush Himalayan extended region (referred to as HKH hereafter), which includes eight major mountain ranges of Hindu Kush, Himalayas, Karakorum, Kunlun, Pamir, Qinling, Tien Shan, and Tibetan Plateau and the associated extensions (Fig. 1). The Hindu Kush Himalayan (HKH) region spans over 4.2 million km^2 (Bajracharya and Shrestha 2011). This region hosts four global biodiversity hotspots and 330 important bird areas (Chaudhary et al., 2022; Chettri et al., 2008). The HKH region directly sustains livelihood of around 240 million people in its mountains and hills, while more than three billion people in its river basins depend on the food produced here (Wester et al., 2019). Hindu-Kush Himalayas have one of the highest mountains in the world with the highest peak of Mount Everest (8848 m) among hundreds of peaks of >6000 m (Wester et al., 2019). This rugged terrain with tropical to alpine climate variation hosts a range of crops, forests types, pastures, flora and fauna (Sharma et al., 2022). The study area was defined using a $1^\circ \times 1^\circ$ degree spatial grid over the HKH high-altitude area, which is subject to perennial snow and ice accumulation.

2.2. Landsat source data

To map the HKH perennial snow and ice cover we employed the Landsat Analysis Ready Data (GLAD ARD) provided by the Global Land Analysis and Discovery team at the University of Maryland (GLAD ARD) (Potapov et al., 2020). GLAD ARD represent a global 16-day normalized surface reflectance dataset from 1997 to 2021. The source data for GLAD ARD were from the Landsat (TM, ETM+, OLI/TIRS) archive provided by the U.S. Geological Survey Earth Resources Observation and Science Centre (USGS EROS). The individual Landsat images were processed to determine per-pixel observation quality. Globally consistent MODIS surface reflectance was used as a normalization target to normalize spectral reflectance. The best clear-sky observations for each 16-day interval were re-

tained creating a consistent 16-day normalized surface reflectance and land surface temperature time-series (Potapov et al., 2020). Here, we employed the GLAD ARD 16-day data for 1997 to 2021, within the HKH region.

The high-altitude and complex terrain of the HKH complicates optical satellite data application due to persistent clouds and both cloud and topographical shadows. Aggregating multiple years instead of annual data increases the number of clear-sky satellite observations in the time-series improving the representation of land surface phenology and enabling identification of perennial snow and ice cover against seasonal snow cover and other land covers. Here, we aggregated Landsat data at five-year epochs. Each five-year epoch consists of the label year and the preceding four years, i.e., 2001 consists of the Landsat data from years 1997–2001, 2006 from 2002 to 2006, 2011 from 2007 to 2011, 2016 from 2012 to 2016, and 2021 from 2017 to 2021. For each epoch, we aggregated the five annual time-series into a single composite time-series by selecting the observation with the highest NDVI values (to prioritize observations with the lowest snow cover) from the five input years for each 16-day interval. Observations contaminated by haze, clouds, and cloud shadows, as indicated by the GLAD ARD quality layer, were removed from the analysis. If no clear-sky data were available for a 16-day interval, we filled the missing reflectance values using linear interpolation with preceding and following intervals.

The 16-day time-series was transformed into a set of multitemporal reflectance metrics, which provides consistent land surface phenology inputs for snow cover mapping (Potapov et al., 2020) (Table 1). For each spectral band, land surface temperature, NDVI (Tucker 1979), NDSI (Bair et al., 2021) and a selection of other normalized ratios between spectral bands (Table 1), we extracted a set of distribution statistics within the 16-day time series for each epoch. Additionally, we ranked the 16-day time-series observations by the corresponding values of NDVI and land surface temperature and then extracted spectral and vegetation index data from the resulting ranking. Some of these metrics, such as spectral reflectance during the peak of the land surface temperature, were key to mapping perennial snow and ice. These metrics showed the land cover during the hottest 16-day interval over the five-year epoch and allowed us to easily discriminate between seasonal and perennial snow cover. Together with the Landsat metrics set, elevation provided by the Shuttle Radar Topography Mission (Reuter et al., 2007) and derived slope, and aspect data were employed as inputs for mapping perennial snow and ice for each epoch.

Table 1
Landsat five-year epoch metrics for mapping perennial show and ice. Q1 and Q3 are quartiles; NIR stands for near infrared, SWIR – shortwave infra-red.

Annual spectral reflectance/index value distribution metrics	
Distribution statistics (*calculated for each spectral band and index value*).	*Spectral bands, physical variables, and index values*
• Minimum •Maximum •Average of all values between minimum and Q1 •Average of all values between Q3 and maximum •Average of all values between Q1 and Q3 •Average of all values	•Blue (482 nm) •Green (561 nm) •Red (654 nm) •NIR (864 nm) •SWIR 1 (1609 nm) •SWIR 2 (2201 nm) •Land surface temperature (K) *Normalized ratios*: •NDVI = (NIR – red)/(NIR + red) •S1N = (NIR – SWIR 1)/(NIR + SWIR1) •S2N = (NIR – SWIR 2)/(NIR + SWIR2) •GR = (green – red)/(green + red) •NDSI = (green – SWIR 1)/(green + SWIR 1)

Annual seasonality metrics		
Distribution statistics (calculated for each spectral band and each distribution method).	Distribution methods (observation dates distributed by the following corresponding indices and values, lowest to highest).	Landsat spectral bands and index values
•Minimum •Maximum •Average of all values between minimum and Q1 •Average of all values between Q3 and maximum	•NDVI = (NIR – red)/(NIR + red) •Land surface temperature (K)	•Blue (482 nm) •Green (561 nm) •Red (654 nm) •NIR (864 nm) •SWIR 1 (1609 nm) •SWIR 2 (2201 nm) Normalized ratios: •S1N = (NIR – SWIR 1)/(NIR + SWIR1) •GS1 = (green – SWIR 1)/(green + SWIR 1)

GLAD ARD quality layer analysis metrics
•Number of clear-sky observations •Water detection proportion •Snow detection proportion

2.3. Image classification

We define the perennial snow and ice class as Landsat 30 m pixels with ≥50% exposed snow or ice cover for all clear-sky observations during the five-year epoch. Pixels where ice presence was obscured due to rocks and debris deposition were not mapped as the perennial snow and ice class. Our definition is similar but not equal to the minimum snow cover, which is observed during summer months (Duo et al., 2014) and has higher variability from year to year.

To calibrate our image classification model, we manually delineated training data of presence and absence of perennial snow and ice using visual image interpretation. We visualized the regional composites of NIR and SWIR spectral reflectance coincident with the per-pixel highest land surface temperature and maximum NDVI to identify the perennial snow and ice cover. To support image interpretation, we used Google Earth time-series high-resolution imagery during the training data collection. To ensure consistent model performance for all epochs, we collected training sites for two epochs, 2001 and 2021, and aggregated them to create a single, year-agnostic model.

The image classification was done using bagged decision tree ensembles (Breiman 1996). To calibrate this supervised classification model, we used binary classes of presence and absence of perennial snow/ice for the 2001 and 2021 epochs as the dependent variable and the corresponding sets of Landsat multi-temporal metrics and topography as independent variables at the spatial resolution of ~30 m (0.00025° × 0.00025°). The decision tree ensemble consisted of 25 tree models. We used a 1% random sample of training data to calibrate each tree model in the ensemble. Each tree model was applied separately to map the perennial snow and ice class likelihood for each Landsat pixel. We then derived the median likelihood from the 25 tree models of the ensemble, and applied a 50% likelihood threshold to create the perennial snow and ice map.

To ensure high quality of the map time-series, we implemented an iterative model calibration approach, also known as active learning. In each classification iteration, we applied the ensemble model calibrated with all training data collected prior to that iteration to the 2001 and 2021 epochs and visually checked the result. Additional training for perennial snow and ice presence and absence were added in each iteration of classification until a satisfactory result was achieved. We then applied the classification model to each of the other three epochs, i.e. 2006, 2011, and 2016, thus creating a five-year epoch time-series of perennial snow and ice maps of the HKH region.

Limited post-processing was applied to remove snow and ice class omissions and commissions within the time-series. Single snow and ice omissions between detections in the time series were considered as class presence. If no snow and ice was detected in both 2001 and 2021 and in less than two consecutive epochs in between, we removed class presence in all epochs. Manual masks to remove map artefacts (e.g., snow overestimation over high altitude glacial lakes and streams) were applied in some regions to improve the map quality.

2.4. Reference sample data

Reference sample data were used to estimate the perennial snow and ice cover area of the total HKH region with associated uncertainty, and to quantify map accuracy for each five-year epoch map. A Landsat pixel (~30 × 30 m, 0.00025° × 0.00025°) was used as a sampling unit. We used a stratified random sampling design to collect reference data. As the perennial snow and ice class is not dominant within the landscape, we selected strata that target the snow and ice presence and change. We also created strata for potential mixed pixels on the boundaries of mapped classes to minimize the effect of map errors on precision of the sample-based estimates (Olofsson et al., 2020). The following strata were created using the 2001–2021 map time-series data: (1) perennial snow/ice absence, core area; (2) perennial snow/ice absence, 30-m periphery; (3) perennial snow and ice, core area; (4) perennial snow and ice, 30-m periphery; (5) loss of perennial snow and ice from 2001 to 2021; (6) gain of perennial snow and ice from 2001 to 2021; (7) all other snow and ice dynamics. From each stratum, we selected randomly 100 pixels for a total of 700 sample pixels.

To collect reference data, we performed visual interpretation of each selected pixel area using available remotely sensed data time-series, including Landsat ARD 16-day data, selected multitemporal metrics, and high-resolution images provided by Google Earth (Fig. 2). In particular, we analyzed all 16-day Landsat ARD composites for the summer months (June to September) and Landsat image composites corresponding to the highest surface temperature values and NDVI over the five-year epoch. A sample pixel was assigned to perennial snow and ice if not even a single snowmelt event was detected during the entire five-year epoch.

2.5. Sample-based area and map accuracy estimation

We estimated the area of perennial snow and ice from the sample reference labels using the equations from Stehman (2014). The sample-based area estimates included perennial snow and ice extent and its loss, gain, and net change for each epoch from 2001 to 2021. All area estimates are provided with their corresponding standard errors (SE) and 95% confidence intervals (CI). The detailed formulae are provided in (Potapov et al., 2022).

From the sample reference labels, we have also estimated map accuracy, including overall accuracy (the estimated proportion of correctly mapped pixels), user's accuracy of the snow and ice class (reflects snow and ice commission) and producer's accuracy of the snow and ice class (reflects snow and ice omission). We used equations from Stehman (2014) to compute these accuracy metrics along with their estimated standard errors (SE).

2.6. Map inter-comparison

We compared our 2021 perennial snow and ice map for HKH with the persistent snow cover layer from the European Space Agency (ESA) 10 m resolution 2021 WorldCover map (Zanaga et al., 2022) created with Sentinel 1 and Sentinel 2 data. The WorldCover map was resampled to a 0.00025° (~30 m) pixel grid using the majority rule (Landsat pixels with ≥50% of snow and ice class

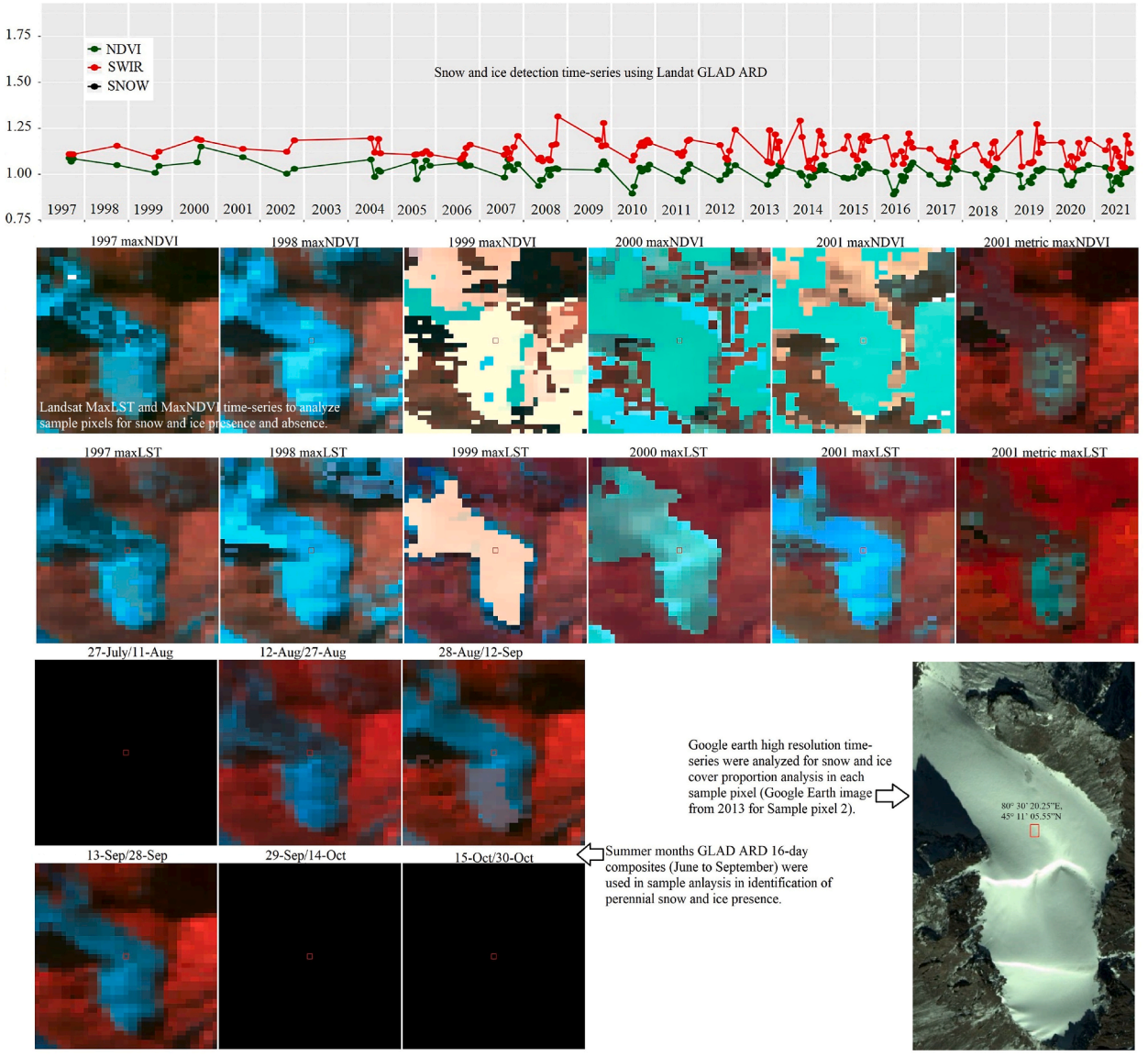

Fig. 2. Example of source reference data for interpretation including time-series plots of NDVI, SWIR1 reflectance and ARD snow detection of valid 16-day interval (top), Landsat image composites surrounding the pixel corresponding to the highest values of land surface temperature (maxLST) and NDVI (maxNDVI) (middle), 16-day composites of summer months (lower left) and Google Earth imagery (lower right). This sample with coordinates 80° 30′ 20.25″E, 45° 11′ 05.55″N was interpreted as perennial snow and ice.

were considered as a reference class). Using our reference sample data, we assessed per pixel accuracy of the ESA World Cover permanent snow and ice layer. We compared the accuracies (overall, producer's and user's) of our map and ESA snow and ice class for the year 2021 (section 3.6).

3. Results

3.1. HKH perennial snow and ice area and change

We mapped perennial snow and ice cover and estimated its area using sample reference data for the HKH region for each of the five epochs, from 2001 to 2021. The resulting regional 30-m perennial snow and ice cover map of stable and change areas is shown in Fig. 3. The map is available for visualization and download (https://glad.earthengine.app/view/snow-ice-hkh).

According to our sample-based area estimates, perennial snow and ice in the HKH region covered 121,705 km^2 (SE = 1645 km^2, 95% CI ± 3224 km^2) in 2001 and 105,935 km^2 (SE = 1732 km^2, CI ± 3396 km^2) in 2021, while the map-based estimates for the two epochs are 122,486 km^2 and 104,715 km^2, respectively (Table 2). Map-based estimates derived using map pixel counts are well within one standard error from the sample-based estimates, indicating that the quality of the map is high enough for area reporting at

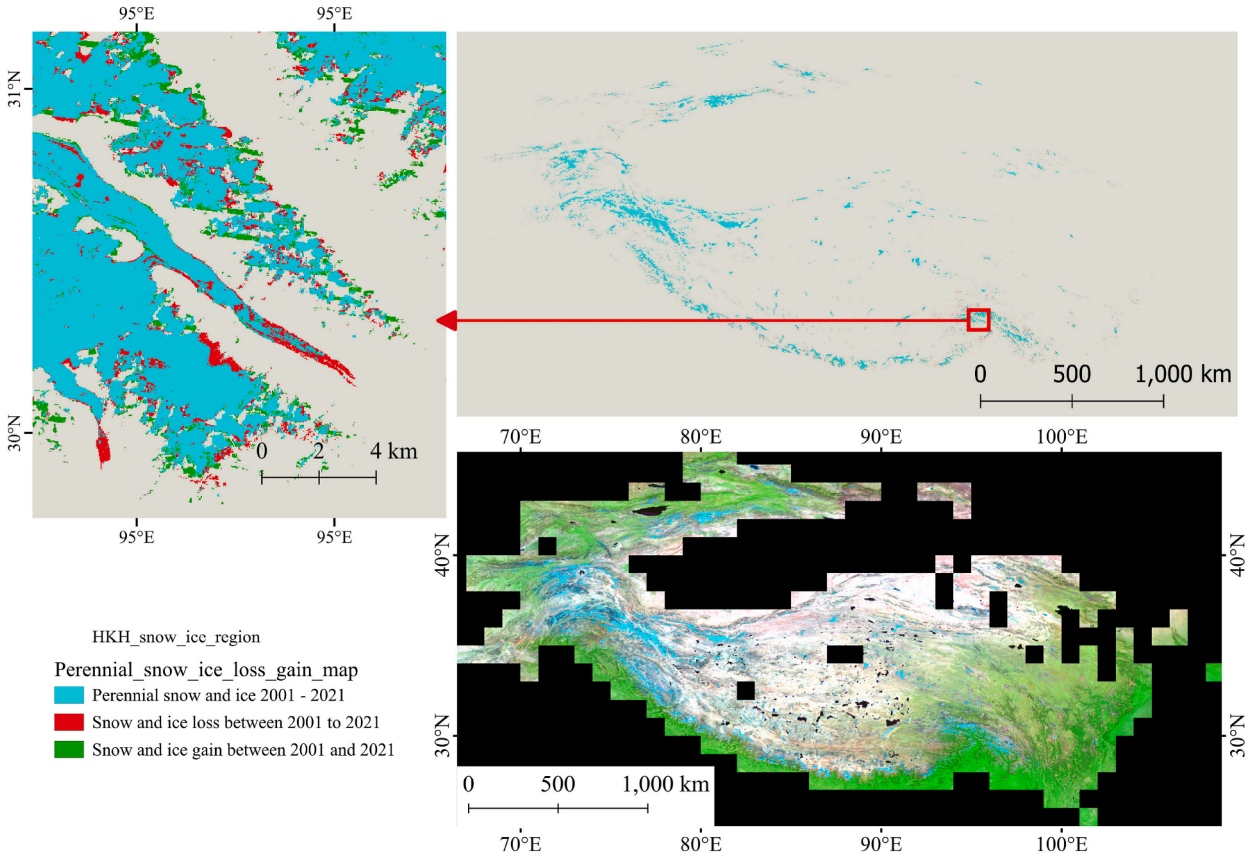

Fig. 3. HKH perennial snow and ice cover map 2021 (above), a random zoomed in region in the HKH (left). Landsat clear-sky image composite for 2021 (below right).

Table 2
Sample-based reference and mapped area estimate for 2001 to 2021.

Year (epoch)	Sample-based perennial snow and ice reference area (km^2) for HKH	Standard Error (SE)	95% Confidence Interval (CI)	Map-based perennial snow and ice area (km^2) for HKH
2001	121,705	1645	3224	122,486
2006	118,827	1671	3275	119,697
2011	114,602	1684	3301	115,537
2016	109,868	1613	3161	108,605
2021	105,935	1732	3396	104,715

the regional level. Assuming the absence of significant sub-regional variations in map quality, we are reporting map-based statistics for individual countries (section 3.3), mountain ranges (section 3.4) and river basins (section 3.5).

At the regional level, both map-based and sample-based area estimates show a reduction of the perennial snow and ice from 2001 to 2021 (Fig. 4). The estimated net loss of the perennial snow and ice area in the HKH region from 2001 to 2021 was 15,770 km^2 (SE = 1630 km^2, 95% CI ± 3195) and 17,770 km^2 using sample and map data, respectively. Average annual net loss of perennial snow and ice for the entire period (between 2001 and 2021), calculated as a mean of the net perennial snow and ice area loss over 21 years, was 751 km^2 (SE = 78 km^2) estimated from the reference sample data. The maximum loss in perennial snow and ice was recorded for the 2011 and 2016 epochs. The slightly higher map-based net loss estimate (outside of one standard error, but within the 95% CI from the sample-based area) is explained by the map-based estimate being higher than the reference sample-based one in 2001 (and the following two epochs) and lower in 2021 (and the preceding epoch) (Table 2). This indicates that the map is slightly more conservative in mapping snow and ice towards the end of the study period compared to the early 2000s.

3.2. Accuracy assessment

The overall accuracy of perennial snow and ice maps for all the five-year epochs was ≥99.5% (Table 3). The user's (UA) and producer's (PA) accuracies of perennial snow and ice cover were high and balanced. UA ranged between 90.9% (SE = 0.05) for 2021 and 94.3% (SE = 1.07) for 2011 and PA between 91.6% (SE = 1.05) for 2021 and 92.8% (SE = 1.18) for 2016.

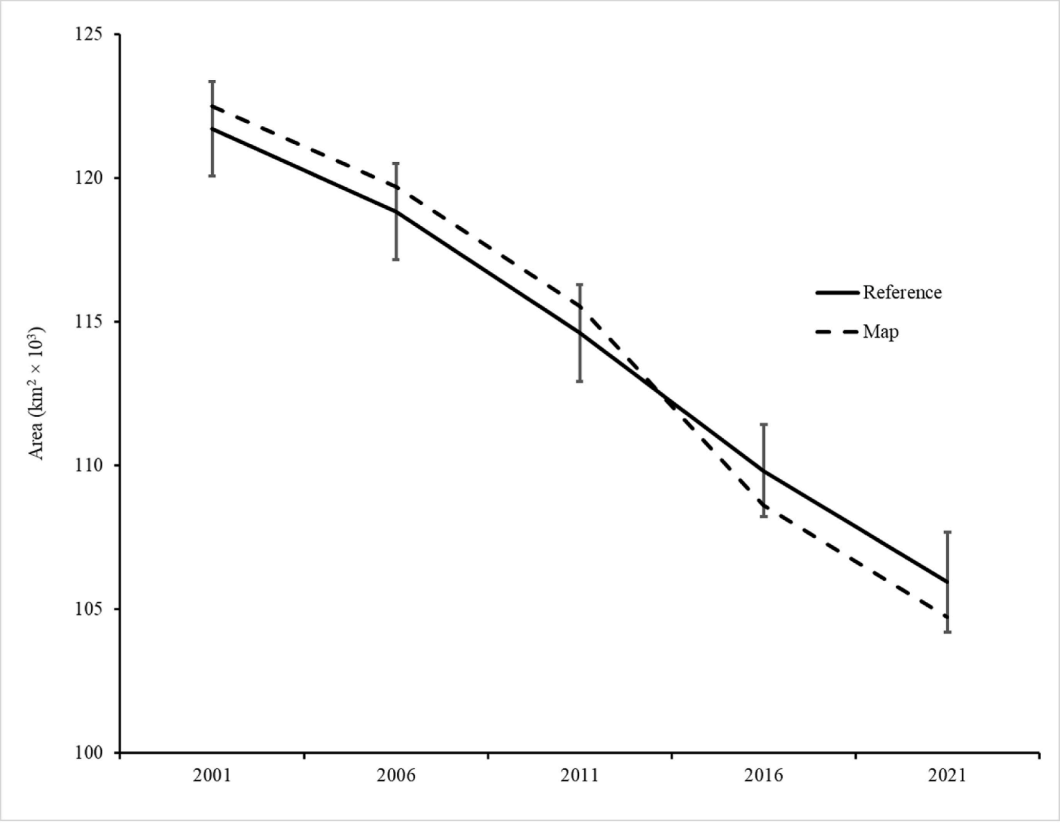

Fig. 4. Perennial snow and ice area estimates for HKH, sample- and map-based. Error bars of the sample-based estimate represent Standard Error.

Table 3
Map accuracies (%) for the five-year epoch perennial snow and ice maps from 2001 to 2021.

Year	Overall accuracy (SE)	User's accuracy (SE)	Producer's accuracy (SE)
2001	99.5 (0.04)	92.3 (1.14)	92.6 (0.95)
2006	99.6 (0.04)	93.0 (1.13)	92.5 (0.97)
2011	99.6 (0.05)	94.3 (1.07)	91.6 (1.21)
2016	99.7 (0.04)	94.3 (1.09)	92.8 (1.18)
2021	99.5 (0.05)	90.9 (1.39)	91.6 (1.05)

We did not perform accuracy assessment at the sub-regional level (e.g. by country, mountain range or river basin). However, the high accuracies (>90% UA and PA for all epochs, Table 3) and closely matching sample- and map-based perennial snow and ice area estimates for all epochs (section 3.1, Table 2 and Fig. 3) at the regional level instil relative confidence in analyzing the distribution of the perennial snow and ice extent and its dynamics by geographic sub-regions within HKH using map data alone.

3.3. Country-level perennial snow and ice cover change in the HKH region

The perennial snow and ice cover in the HKH region is shared among 11 countries. China contains 47% of the total 2021 perennial snow and ice cover, followed by Pakistan with 15% and India with 14% (Table 4), while Kazakhstan, Uzbekistan, and Myanmar have 1% or less each. China also has the largest contribution to the total net loss of perennial snow and ice cover of the HKH (8464 km^2), followed by India and Pakistan. Among the countries with at least 1000 km^2 of perennial snow and ice cover, Nepal had the highest 2001–2021 net perennial snow and ice reduction rate of 31%, followed by Kyrgyzstan and India (22% reduction rate each).

3.4. Mountain range-level snow and ice cover change in the HKH region

All of the mountain ranges in the HKH experienced a net loss in its perennial snow and ice cover from 2001 to 2021 (Fig. 5). The largest loss in terms of both area and rate of change was found in Tibetan plateau, with the net reduction of perennial snow and ice of 4050 km^2 (22% of the year 2001 area). The perennial snow and ice area in Karakorum, Tien Shan, Western and Central Himalayas reduced by at least 10% during the last two decades. The western mountain ranges including Kunlun, Hindu Kush, and Karakorum have a slight increase in perennial snow cover in 2006 against 2001 but experienced a reduction of the cover after 2006.

Table 4
Country-level distribution of the perennial snow and ice cover in the HKH region. The table shows map-based areas.

Country	Perennial snow and ice area for the year 2001, km^2	Percent of the total area of 2001 perennial snow and ice in the HKH region	Perennial snow and ice area for the year 2021, km^2	Percent of the total area of 2021 perennial snow and ice in the HKH region	Net change of perennial snow and ice, km^2	Percent net change of the year 2001 (%)
Afghanistan	3047	2.5	2609	2.5	−438	(2.5)
Bhutan	1458	1.2	1269	1.2	−189	(1.1)
China	58,616	47.9	50,152	47.9	−8464	(47.6)
India	18,140	14.8	15,048	14.4	−3092	(17.4)
Kazakhstan	1162	1.0	1075	1.0	−87	(0.5)
Kyrgyzstan	7129	5.8	5886	5.6	−1243	(7.0)
Myanmar	166	0.1	244	0.2	78	0.4
Nepal	5955	4.9	4610	4.4	−1345	(7.6)
Pakistan	16,972	13.9	15,379	14.7	−1593	(9.0)
Tajikistan	9738	8.0	8372	8.00	−1366	(7.7)
Uzbekistan	103	0.1	71	0.1	−32	(0.2)

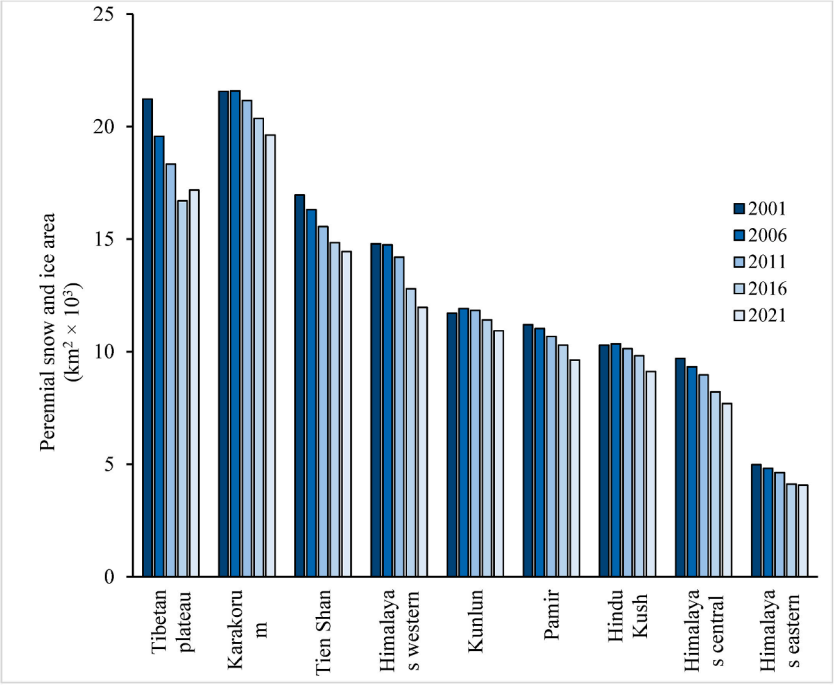

Fig. 5. Mountain range-level change in perennial snow and ice cover from map-based areas for each of the major mountain ranges in the HKH region estimated.

3.5. River basin-level perennial and ice cover change in the HKH

Among the HKH major river basins, Indus River basin has the largest perennial snow and ice cover in 2021, followed by Brahmaputra and Tarim (Table 5). During 2001–2021 period, the Indus River basin lost 4119 km^2 (13% of the year 2001 area) of its perennial snow and ice cover. Among river basins with at least 1000 km^2 perennial snow and ice area, Salween, Yangtze, Ganges, and Brahmaputra experienced the highest snow and ice reduction rates of 35%, 23%, 21% and 18%, respectively.

3.6. Comparison with ESA WorldCover

The mapped area of ESA World Cover's snow and ice class for the HKH region is 20% higher than our area estimate using the reference sample data and 21% higher than our mapped area for 2021. The accuracy assessment of the ESA World Cover's snow and ice class employing our sample reference data shows an overall accuracy of 99.2% (SE = 0.06), not significantly different than our 99.5% (SE = 0.05) for the year 2021. However, the ESA user's and producer's accuracies of 84.9% (SE = 1.28) and 86.9% (SE = 2.1) are lower than the 90.9 % (SE = 1.39) user's and 91.6% (SE = 1.05) producer's accuracies of our 2021 permanent snow and ice map for the HKH.

We performed visual analysis of disagreement between our map of perennial snow and ice cover and the ESA World Cover product. Based on this qualitative visual map inter-comparison, we found four major reasons for the disagreement between the two perennial snow and ice maps (Fig. 6,Fig. 7). First, the ESA WorldCover omitted perennial snow and ice in mountain shadows and deep narrow valleys. Our perennial snow and ice map for 2021 performs better in mapping perennial snow and ice in such areas (Fig. 6c). Sec-

Table 5
Basin-level perennial snow and ice cover of HKH. The table shows the map-based areas.

River Basin	2001 Perennial snow and ice area for the year 2001, km^2	Percent of the total area of 2001 perennial snow and ice in the HKH region	2021 Perennial snow and ice area for the year 2021, km^2	Percent of the total area of 2021 perennial snow and ice in the HKH region	Net change of perennial snow and ice, km^2	Percent net change of the year 2001 (%)
Indus	31,492	27.3	27,373	27.8	−4119	(24.7)
Tarim	29,727	25.8	27,111	27.5	−2616	(15.7)
Brahmaputra	17,296	15.0	14,248	14.5	−3048	(18.3)
Aral	15,427	13.4	12,948	13.1	−2479	(14.9)
Ganges	12,201	10.6	9654	9.8	−2547	(15.3)
Balkhash	2881	2.5	2539	2.6	−342	(2.1)
Yangtze	2193	1.9	1698	1.7	−495	(3.0)
Salween	2192	1.9	1432	1.5	−760	(4.6)
Issykul	593	0.5	514	0.5	−79	(0.5)
Chuy	482	0.4	380	0.4	−102	(0.6)
Mekong	312	0.3	209	0.2	−103	(0.6)
Irawaddy	188	0.2	271	0.3	83	0.5
Yellow	172	0.2	146	0.2	−26	0.2
Talas	76	0.1	57	0.1	−19	0.1

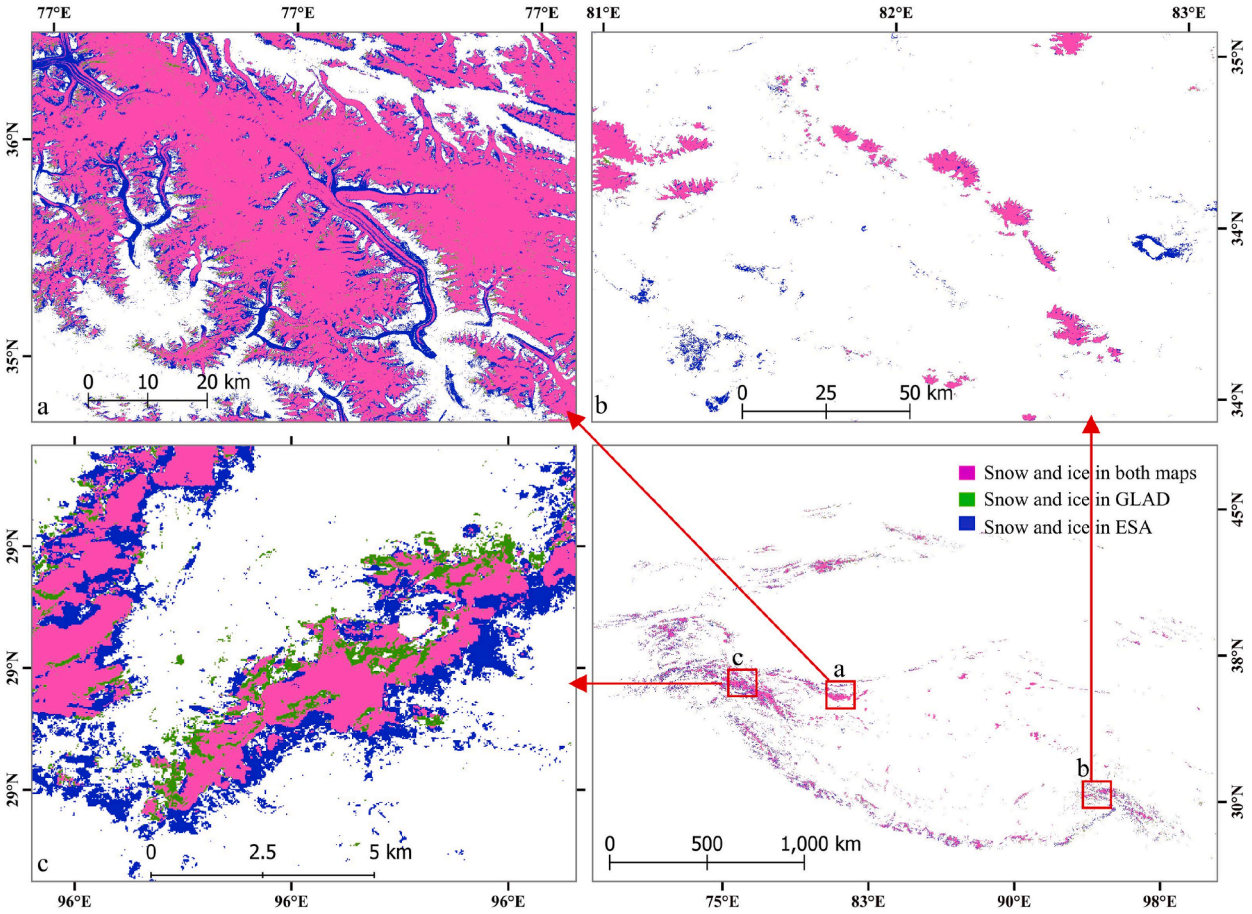

Fig. 6. Comparison of commission and omission errors between ESA WorldCover map persistent snow (2021) and GLAD 2021 perennial snow and ice map. a. Example of glacier area underestimation by GLAD product due to debris over ice. b. Overestimation of snow and ice by ESA map over lakes. c. Examples of errors in ESA map over seasonal snow (overestimation) and shadows (underestimation).

ond, our product underestimated the glacier area when the snow and ice was covered by debris. ESA employed Sentinel-1 radar data that are able to penetrate under the surface of the debris to detect ice and more successfully mapped debris-covered glacial area (Figs. 6a and 7). The inability to map ice under rocks and debris is the major drawback of using Landsat optical data. The third reason is the overestimation of perennial snow and ice cover by the WorldCover product due to the inclusion of seasonal snow cover (Fig. 6c). Finally, we found that salt lakes and salt pans were commonly incorrectly mapped as snow cover by the WorldCover product (Fig. 6b).

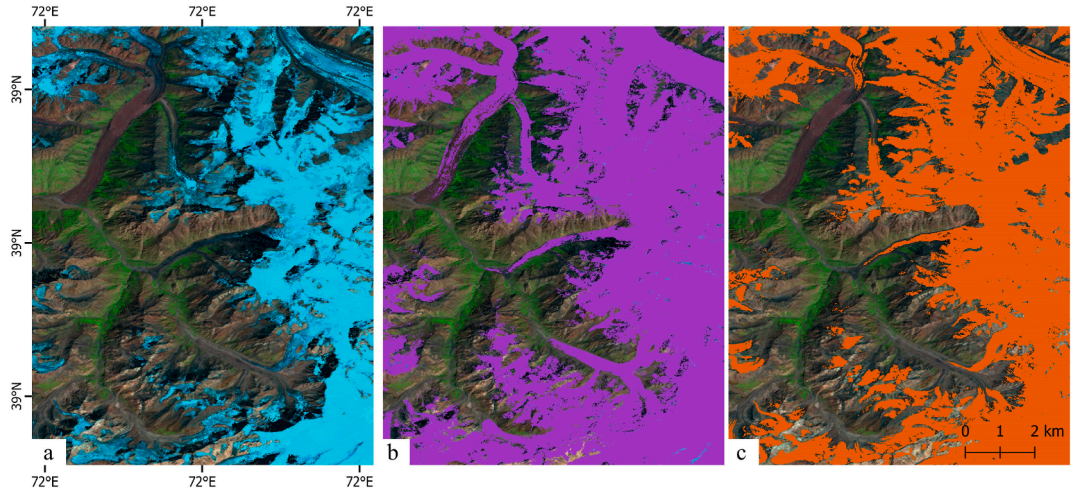

Fig. 7. a - Landsat composite during the highest land surface temperature for the 2021 epoch, with exposed snow and ice cover – appearing light blue; b – ESA WorldCover 2021 snow and ice cover layer 2021; c - GLAD HKH perennial snow and ice map for 2021.

Based on the visual map analysis, we suggest that our perennial snow and ice map has higher accuracy outside of debris-covered glaciers compared to the ESA WorldCover.

4. Discussion

4.1. Challenges of regional scale mapping of perennial snow and ice cover

Deriving accurate land cover statistics in the high mountains with either conventional field-based methods or through satellite remote sensing is challenged by a range of factors. Rugged topography and remoteness are major constraints to field-based data collection. Mapping of snow and ice cover extent and its temporal dynamics with optical satellite imagery is difficult due to the observation contamination by clouds and mountain shadows, and spectral similarity of snow with high-altitude glacial lakes, salt pans, clouds, and bright rocks. The capability to process large volumes of high spatial and temporal resolution remote sensing data is another challenge for regional-scale multidecadal monitoring. Therefore, monitoring of snow and ice cover in the HKH was traditionally limited to localized mapping with a focus restricted to glaciers in parts of the HKH region and to coarse resolution satellite datasets such as AVHRR and MODIS (Bajracharya and Shrestha 2011; Desinayak et al., 2022; Duo et al., 2014; Gurung et al., 2011b; Hall et al., 2006; Immerzeel 2008; Pandey et al., 2011; Pratibha and Kulkarni 2018). At the regional scale, ICIMOD (Gurung et al., 2011b) employed MODIS-derived snow detection to map snow and ice in the HKH region. ESA has created a global land cover map at 10 m spatial resolution using Sentinel 1 and Sentinel 2 data with a persistent snow/ice cover as part of the WorldCover product (Zanaga et al., 2022). However, the WorldCover product does not provide a perspective on a multidecadal change of snow and ice cover in the HKH region and the commission errors of the WorldCover snow and ice map are significant within the HKH region (see section 3.6).

4.2. Significance of GLAD Landsat ARD to map perennial snow and ice at a regional scale

In this research, we employed 30 m Landsat ARD 16-day composites since 1997 aggregated by five-years epochs. The long intervals for each epoch were used to overcome data gaps, which are common in the Landsat dataset for this mountainous high-altitude region with frequent cloud cover. The data gaps are specifically an issue for Landsat 5 and 7 archives, when only a limited number of image acquisitions per year were recorded (Ju and Roy 2008). Although constrained by the image availability, this legacy data provides an opportunity to assess the spatial extent of a land cover such as the perennial snow and ice in HKH, and estimate change over time. Overall, 190,328 Landsat scenes from 1997 to 2021 were processed to create the GLAD ARD that were employed for regional snow and ice mapping. The GLAD ARD provided unique pre-processed inputs for regional and global land cover and change mapping. Unprecedented high Landsat 8 and 9 observation frequency since 2021 supports frequent (annual or bi-annual) snow and ice monitoring in the future (Masek et al., 2020). The main shortcoming of the optical data is the inability to detect ice under rocks and debris. Adding radar time-series data, such as Sentinel-1, may help improving future glacier monitoring capabilities of the presented method.

4.3. Changes in the perennial snow and ice in the HKH region

Earlier studies, regardless of the method used, agree that the HKH region has lost significant snow and ice cover over the past few decades, particularly under the rising global temperatures. According to projections by IPCC, the HKH region will lose its snow and ice cover and particularly small glaciers will disappear by 2030 (IPCC et al., 2007). Both our sample-based analysis and our Landsat-based map time-series confirms a consistent decline in the perennial snow cover in the HKH region during the last two decades.

We suggest that the observed reduction of perennial snow and ice is a direct response to the recent increase in annual temperatures in the region. A significant increase at the rate of 0.28 °C per decade in the mean annual surface air temperature is recorded in the HKH between 1951 and 2020 (Wester et al., 2023). Snow melt has a direct correlation with temperature variability (IPCC 2022),

thus increasing temperature trends would mean higher melting rates and longer ablation periods. Our study provides a basis to assess the climate change impacts and its severity in the region with over 3 billion people, around one fourth of the world's total population. The large river systems such as Indus, Brahmaputra, Ganges, Yangtze, and Yellow that originate in the HKH mountain systems have played key socio-economic role for the regional populations. An imbalance in the hydrological processes' dependent on snow and ice melt in the HKH will have a profound impact on the lives of the people living in these river basins. Presented perennial snow and ice map time-series and the monitoring method support the assessment of how climate change impacts the regional population. Our data provide input for policy makers seeking to achieve food and water security for the world's most populated river basins.

5. Conclusion

There is evidence of changing cryosphere in the HKH region and elsewhere in the world, yet quantitative estimates suffer from high uncertainties (Wilson et al., 2017). Here, we document a ±13% net decline in the area of perennial snow and ice from 2001 to 2021 in the HKH region, with 105,935 km^2 (SE ± 1732 km^2) remaining in 2021. We employed a consistently processed Landsat ARD aggregated over a five-year epoch to create a consistent map of perennial snow and ice change at a regional scale. The five-year epochs were chosen to overcome data limitations and increase mapping precision. The presented method allowed highly accurate quantification of perennial snow and ice change over the past twenty years. Our products were validated using reference sample data and found highly reliable with user's and producer's accuracies of the target class over 90%. Our results confirmed the declining snow cover in the HKH region and demonstrated the suitability of GLAD ARD product for multidecadal mapping of perennial snow and ice change at a large geographic extent. The global-scale application of our method will support perennial snow and ice cover change area monitoring under the ongoing climate change.

Declaration of interest statement: The authors declare no conflict of interest.

Ethical statement

The presented study is based on publicly available satellite imagery and employed open-source and open-access GIS software. The work was supported by the Global Land Analysis and Discovery Lab (GLAD) at the University of Maryland. The funding for the GLAD lab comes from private and state research funds, including Bezos Earth Fund, the WRI Global LCLU Monitoring Program (#G2436), the NASA/USGS Landsat Science Team (#140G0118C0013), and the NASA SERVIR program (#80NSSC20K0158). No direct financial support or consulting fees were received by the authors.

CRediT authorship contribution statement

Ahmad Khan: Formal analysis, Visualization, Writing – original draft, Writing – review & editing. **Peter Potapov:** Conceptualization, Data curation, Methodology, Software, Visualization, Writing – review & editing. **Matthew C. Hansen:** Conceptualization, Funding acquisition, Supervision. **Amy H. Pickens:** Visualization, Writing – review & editing. **Alexandra Tyukavina:** Validation, Writing – review & editing. **Andres Hernandez Serna:** Software, Visualization. **Kabir Uddin:** Validation. **Jawairia Ahmad:** Writing – review & editing.

Declaration of competing interest

The authors declare that they have no known competing financial interests or personal relationships that could have appeared to influence the work reported in this paper.

Data availability

ARD data employed in this research is publicly available free of cost from glad.umd.edu.

Acknowledgements

This study was supported by the Bezos Earth Fund, the WRI Global LCLU Monitoring Program (#G2436), the NASA/USGS Landsat Science Team (#140G0118C0013), and the NASA SERVIR program (#80NSSC20K0158). The authors would like to thank Svetlana Turubanova (GLAD UMD), Alexander Krylov (former GLAD UMD), Qing Ying (ESSIC UMD) and Bernard Adusei (GLAD UMD) for their help with GLAD ARD production.

References

Archer, D., 2003. Contrasting hydrological regimes in the upper Indus Basin. J. Hydrol. 274, 198–210.
Archer, D.R., 2001. The climate and Hydrology of northern Pakistan with respect to assessment of flood risk to hydropower schemes. In: Lahore:: German Technical Cooperation Agency (GTZ) and Water and Power Development Authority (WAPDA).
Bair, E.H., Stillinger, T., Dozier, J., 2021. Snow property inversion from remote sensing (SPIReS): a generalized multispectral unmixing approach with examples from MODIS and Landsat 8 OLI. IEEE Trans. Geosci. Rem. Sens. 59, 7270–7284.
Bajracharya, S., Shrestha, B. (Eds.), 2011, The Status of Glaciers in the Hindu Kush-Himalayan Region. ICIMOD, Kathmandu.
Bolch, T., Kulkarni, A., Kaab, A., Huggel, C., Paul, F., Cogley, J.G., Frey, H., Kargel, J.S., Fujita, K., Scheel, M., Bajracharya, S., Stoffel, M., 2012. The state and fate of himalayan glaciers. Science 336, 310–314.
Bookhagen, B., Burbank, D.W., 2010. Toward a complete Himalayan hydrological budget: spatiotemporal distribution of snowmelt and rainfall and their impact on river discharge. Journal of Geophysical Research Earth Surface 115, 1–25.
Breiman, L., 1996. Bagging predictors. Mach. Learn. 24, 123–140.

Brown, R.D., 2000. Northern hemisphere snow cover variability and change, 1915–97. J. Clim. 13, 2339–2355.
Chaudhary, S., Uddin, K., Chettri, N., Thapa, R., Sharma, E., 2022. Protected areas in the Hindu Kush Himalaya: a regional assessment of the status, distribution, and gaps. Conservation Science and Practice 4, e12793.
Chettri, N., Shakya, B., Thapa, R., Sharma, E., 2008. Status of a protected area system in the Hindu Kush-Himalayas: an analysis of PA coverage. Int. J. Biodivers. Sci. Manag. 4, 164–178.
Cogley, J.G., 2016. Glacier shrinkage across high mountain asia. Ann. Glaciol. 57, 41–49.
Desinayak, N., Prasad, A.K., El-Askary, H., Kafatos, M., Asrar, G.R., 2022. Snow cover variability and trend over the Hindu Kush Himalayan region using MODIS and SRTM data. Ann. Geophys. 40, 67–82.
Duo, C., Xie, H., Wang, P., Guo, J., La, J., Qiu, Y., Zheng, Z., 2014. Snow cover variation over the Tibetan Plateau from MODIS and comparison with ground observations. Journal of Applied Remote Sesning (8).
Dyurgerov, M.B., Meier, M.F., 2005. Glaciers and the changing earth system - a 2004 snapshot. In: Colorado: Institute of Arctic and Alpine Research. University of Colorado, Boulder, Colorado.
Erickson, J.D., 1984. The LACIE experiment in satellite aided monitoring of global crop production. In: Goodwell, G.M. (Ed.), The Role of Terrestrial Vegetation in the Global Carbon Cycle: Measurement by Remote Sensing. John Wiley & Sons Ltd, New York, USA, pp. 191–217.
Gurung, D.R., Kulkarni, A.V., Giriraj, A., Aung, K.S., Shrestha, B., Srinivasan, J., 2011a. Changes in seasonal snow cover in Hindu Kush-Himalayan region. Cryosphere Discuss. 2011, 755–777.
Gurung, D.R., Kulkarni, A.V., Giriraj, A., San Aung, K., Shrestha, B., 2011b. Monitoring of seasonal snow cover in Bhutan using remote sensing technique. Curr. Sci. 101, 1364–1370.
Hall, D.K., Riggs, G.A., Salomonson, V.V., 2006. MODIS snow and sea ice products. Earth Science Satellite Remote Sensing: Science and Instruments 1, 154.
Hall, D.K., Riggs, G.A., Salomonson, V.V., DiGirolamo, N.E., Bayr, K.J., 2002. MODIS snow-cover products. Rem. Sens. Environ. 83, 181–194.
Immerzeel, W., 2008. Historical trends and future predictions of climate variability in the Brahmaputra basin. Int. J. Climatol. 28, 243–254.
Immerzeel, W.W., Beek, L.P.H.v., Bierkens, M.F.P., 2010. Climate change will affect the asian water towers. Science 328, 1382–1385.
Immerzeel, W.W., Droogers, P., de Jong, S.M., Bierkens, M.F.P., 2009. Large-scale monitoring of snow cover and runoff simulation in Himalayan river basins using remote sensing. Rem. Sens. Environ. 113, 40–49.
IPCC, 2007. In: Soloman, S., Qin, D., Manning, M., Chen, Z., Marquis, M., Averyt, K., Tignor, M., Miller, H. (Eds.), The Physical Science Basis: Contribution of Working Group I to the Fourth Assessment Report of the Intergovernmental Panel on Climate Change. Cambridge University Press, Cambridge, United Kingdom and New Yor, NY, USA, p. 996.
IPCC, 2022. Climate Change 2022: Impacts, Adaptation and Vulnerability Sixth Assessment Report of the Intergovernmental Panel on Climate Change. (Cambridge, UK and New York, NY, USA).
IPCC, 2022b. Summary for policy makers. In: Pörtner, H.-O., Roberts, D.C., Poloczanska, E.S., Mintenbeck, K., Tignor, M., Alegría, A., Craig, M., Langsdorf, S., Löschke, S., Möller, V., Okem, A. (Eds.), Climate Change 2022: Impacts, Adaptation, and Vulnerability. Contribution of Working Group II to the Sixth Assessment Report of the Intergovernmental Panel on Climate Change. Cambridge University Press, UK and New York, USA.
Ju, J., Roy, D.P., 2008. The availability of cloud-free Landsat ETM+ data over the conterminous United States and globally. Rem. Sens. Environ. 112, 1196–1211.
Lee, E., Carrivick, J.L., Quincey, D.J., Cook, S.J., James, W.H.M., Brown, L.E., 2021. Accelerated mass loss of himalayan glaciers since the little ice age. Sci. Rep. 11, 24284.
Lindsey, R., Dahlman, L., Blunden, J., 2023. Climate Change: Global Temperature. NOAA. https://www.climate.gov/news-features/understanding-climate/.
Masek, J.G., Wulder, M.A., Markham, B., McCorkel, J., Crawford, C.J., Storey, J., Jenstrom, D.T., 2020. Landsat 9: empowering open science and applications through continuity. Rem. Sens. Environ. 248, 111968.
Matson, M., Ropelewski, C.F., Varnadore, M.S., United States National Environmental Satellite Data Information Service, & United States National Weather Service, 1986. NOAA Atlas : an atlas of satellite-derived northern hemispheric snow cover frequency. In: U.S. Dept. Of Commerce, National Oceanic and Atmospheric Administration, National Environmental Satellite, Data, and Information Service. National Weather Service, Washington, DC.
NASA, 2023. World of Change: Global Temperatures. https://earthobservatory.nasa.gov/world-of-change/global-temperatures. (NASA Earth Observatory).
Olofsson, P., Arévalo, P., Espejo, A.B., Green, C., Lindquist, E., McRoberts, R.E., Sanz, M.J., 2020. Mitigating the effects of omission errors on area and area change estimates. Rem. Sens. Environ. 236, 111492.
Owen, L.A., Finkel, R.C., Caffee, M.W., 2002. A note on the extent of glaciation throughout the Himalaya during the global Last Glacial Maximum. Quat. Sci. Rev. 21, 147–157.
Pandey, P.K., Frey, K.E., Ghimire, B., 2011. Detection of the timing and durationof snowmelt in the Hindu Kush-Himalaya using QuikSCAT. Environ. Res. Lett. 6, 2000–2008.
Peng, X., Frauenfeld, O.W., Jin, H., Du, R., Qiao, L., Zhao, Y., Mu, C., Zhang, T., 2021. Assessment of temperature changes on the Tibetan plateau during 1980–2018. Earth Space Sci. 8, e2020EA001609.
Potapov, P., Hansen, M.C., Kommareddy, I., Kommareddy, A., Turubanova, S., Pickens, A., Adusei, B., Tyukavina, A., Ying, Q., 2020. Landsat analysis ready data for global land cover and land cover change mapping. Rem. Sens. 12.
Potapov, P., Turubanova, S., Hansen, M.C., Tyukavina, A., Zalles, V., Khan, A., Song, X.-P., Pickens, A., Shen, Q., Cortez, J., 2022. Global maps of cropland extent and change show accelerated cropland expansion in the twenty-first century. Nature Food 3, 19–28.
Pratibha, S., Kulkarni, A.V., 2018. Decadal change in supraglacial debris cover in Baspa basin, Western Himalaya. Curr. Sci. 114, 792–799.
Racoviteanu, A.E., Paul, F., Raup, B., Khalsa, S.J.S., Armstrong, R., 2009. Challenges and recommendations in mapping of glacier parameters from space: results of the 2008 Global Land Ice Measurements from Space (GLIMS) workshop, Boulder, Colorado, USA. Ann. Glaciol. 50, 53–69.
Ramamoorthi, A.S., Haefner, H., 1991. Runoff modeling and forecasting of river basins, and himalayan snowcover information (HIMSIS). In: Vienne Symposium, IAHS. p. 9.
Remy, F., Flament, T., Blarel, F., Benveniste, J., 2012. Radar altimetry measurements over antarctic ice sheet: a focus on antenna polarization and change in backscatter problems. Adv. Space Res. 50, 998–1006.
Ren, Y.-Y., Ren, G.-Y., Sun, X.-B., Shrestha, A.B., You, Q.-L., Zhan, Y.-J., Rajbhandari, R., Zhang, P.-F., Wen, K.-M., 2017. Observed changes in surface air temperature and precipitation in the Hindu Kush Himalayan region over the last 100-plus years. Adv. Clim. Change Res. 8, 148–156.
Reuter, H.I., Nelson, A., Jarvis, A., 2007. An evaluation of void-filling interpolation methods for SRTM data. Int. J. Geogr. Inf. Sci. 21, 983–1008.
Rikiishi, K., Nakasato, H., 2006. Height dependence of the tendency for reduction in seasonal snow cover in the Himalaya and the Tibetan Plateau region, 1966–2001. Ann. Glaciol. 43, 369–377.
Sharma, U.C., Datta, M., Sharma, V., 2022. Introduction. In: Sharma, U.C., Datta, M., Sharma, V. (Eds.), Soils in the Hindu Kush Himalayas: Management for Agricultural Land Use. Springer International Publishing, Cham, pp. 1–25.
The Himalayan Climate and Water Atlas: impact of climate change on water resources in five of Asia's major river basins. In: Shrestha, A., Agarwal, N., Alfthan, B., Barjracharya, S., Marechal, J., van Oort, B. (Eds.), 2015, ICIMOD, GRID-Arendal and CICERO.
Shrestha, A.B., Camerson, P.W., Mayewski, P.A., Dibb, J.E., 1999. Maximum temperature trends in the Himalaya and its vicinity: an analysis based on temperature records from Nepal for the period 1971-1994. J. Clim. 12.
Stehman, S.V., 2014. Estimating area and map accuracy for stratified random sampling when the strata are different from the map classes. Int. J. Rem. Sens. 35, 4923–4939.
Trishchenko, A.P., Ungureanu, C., 2021. Minimum snow/ice extent over the northern circumpolar landmass in 2000–19: how much snow survives the summer melt? Bull. Am. Meteorol. Soc. 102, E748–E764.
Tucker, C.J., 1979. Photographic infrared linear combinations for monitoring vegetation. Rem. Sens. Environ. 8 (2), 127–150.
Viste, E., Sorteberg, A., 2015. Snowfall in the Himalayas: an uncertain future from a little-known past. Cryosphere 9, 1147–1167.
Wang, W., Huang, X., Deng, J., Xie, H., Liang, T., 2015. Spatio-temporal change of snow cover and its response to climate over the Tibetan plateau based on an improved daily cloud-free snow cover product. Rem. Sens. 7, 169–194.

Wang, X., Xie, H., 2009. New methods for studying the spatiotemporal variation of snow cover based on combination products of MODIS Terra and Aqua. J. Hydrol. 371, 192–200.
Wester, P., Chaudhary, S., Chettri, N., Jackson, M., Maharjan, A., Nepal, S., Steiner, J.F., 2023. Water, Ice, Society, and Ecosystems in the Hindu Kush Himalaya: an Outlook. International Centre for Integrated Mountain Development, Kathmandu, Nepal.
Wester, P., Mishra, A., Mukherji, A., Shreshta, A.B. (Eds.), 2019, The Hindu Kush Himalaya Assessment - Mountains, Climate Change, Sustainability and People. Springer Nature Switzerland AG, Cham, Switzerland.
Wilson, A.M., Gladfelter, S., Williams, M.W., Sonika, S., Prashant, B., Richard, A., Adina, R., 2017. High Asia: the international dynamics of climate change and water security. J. Asian Stud. 76, 24.
WorldBank, 2023. Development Indicators. World Bank.
Zanaga, D., Van De Kerchove, R., Daems, R., Keersmaecker, W.D., Brockmann, C., Kirches, G., Wevers, J., Cartus, O., Santoro, M., Fritz, S., Lesiv, M., Herold, M., Tsendbazar, E., Xu, P., Ramoino, F., Arino, O., 2022. ESA WorldCover 10 m 2021 v200. In: worldcover2021.esa.int. European Space Agency.
Zhou, Y., Dong, J., Liu, J., Metternicht, G., Shen, W., You, N., Zhao, G., X, X., 2019. Are there sufficient Landsat observations for retrospective and continuous monitoring of land cover changes in China? Rem. Sens. 11.